Published in : Journal of Material Chemistry A (2019), vol. 14, pp. 8226–8233
DOI: 10.1039/C9TA00116F
Status : Postprint (Author's version)

SODIUM IRON SULFATE ALLUAUDITE SOLID SOLUTION FOR Na-ION BATTERIES: MOVING TOWARDS STOICHIOMETRIC $Na_2Fe_2(SO_4)_3$

Thomas Jungers,[a] Abdelfattah Mahmoud,[a] Cedric Malherbe,[b] Frederic Boschini[a] and Benedicte Vertruyen[a]

[a] *GREENMAT, CESAM Research Unit, University of Liège, 4000 Liège, Belgium.*
[b] *Laboratory of Inorganic Analytical Chemistry, MolSys Research Unit, University of Liege, 4000 Liege, Belgium*

Abstract

Thanks to the inductive effect of the sulfate groups, sodium iron sulfate alluaudites display the highest electrode potential amongst the Fe-based compounds studied in sodium-ion batteries. Here, we report the synthetic strategy that has allowed us to obtain the elusive $Na_2Fe_2(SO_4)_3$ stoichiometric compound through a reverse-strike coprecipitation method in organic medium. We experimentally confirm the hypothesis that the stoichiometric compound transforms upon further heat treatment into the previously reported sodium-rich solid solution and an iron sulfate secondary phase. X-ray diffraction and ^{57}Fe Mössbauer spectroscopy do not reveal any striking structure difference between the stoichiometric and Na-rich compounds, in agreement with the current understanding that the instability of the stoichiometric phase is due to the repulsion between Fe^{2+} ions in the Fe_2O_{10} dimers bridged by sulfate groups. Despite less-than-optimal powder microstructure, electrochemical activity of the stoichiometric phase could be demonstrated through operando X-ray diffraction. These findings are expected to shift attention towards the (near)-stoichiometric compositions, which offer the highest theoretical specific capacities thanks to their optimal Na/Fe ratio.

Introduction

The increasing contribution of intermittent renewable energies to the global market drives the need for sustainable means of energy storage. In this context, the low cost, high abundance and broad geographical distribution of sodium and iron stimulate the interest for Na-ion batteries with Fe-based positive electrode materials. Amongst these, preference is obviously given to the compounds offering the highest energy density.

Sodium iron sulfate $Na_{2+2x}Fe_{2-x}(SO_4)_3$ (NFS) was first reported in 2014.[1] Thanks to the high electronegativity of the sulfate groups, an inductive effect[2] raises the reduction potential of the

Published in : Journal of Material Chemistry A (2019), vol. 14, pp. 8226–8233
DOI: 10.1039/C9TA00116F
Status : Postprint (Author's version)

Fe^{3+}/Fe^{2+} couple to ~3.8 V vs. Na^+/Na^0. This value of potential is the highest reported for the Fe^{3+}/Fe^{2+} couple[1,3] and is combined with a theoretical specific capacity of ~120 mA h g^{-1} if $x = 0$.[4] Unlike most $A_2M_2(XO_4)_3$ compounds, which crystallize in a NASICON structure,[5–7] NFS displays an alluaudite-type structure (Fig. 1) with large channels favoring fast diffusion of sodium ions.[1,4,5,8–11]

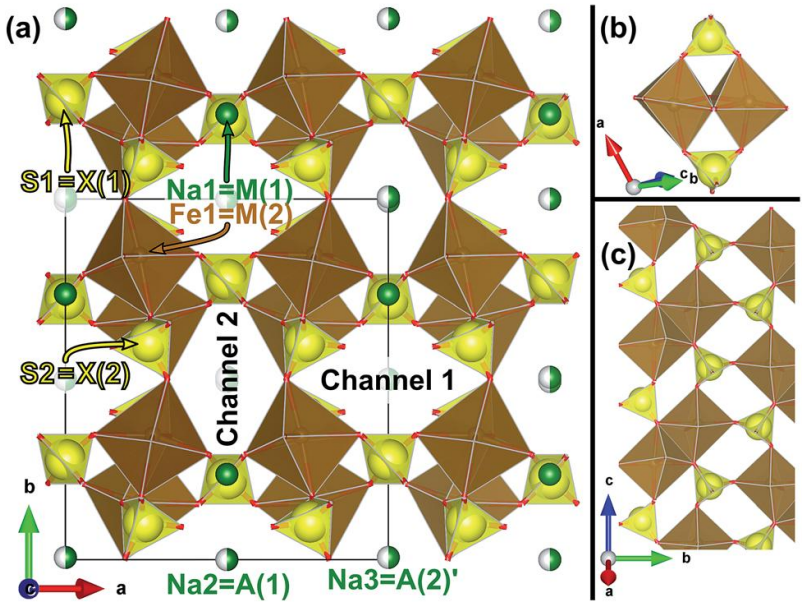

Fig. 1 *(a) Alluaudite structure (C2/c space group). Fe atoms are represented in brown, Na in green, S in yellow andOin red. The figure also shows the labels used in the Rietveld refinements (Tables S1-3 and S1- 4 in ESI). (b) Dimers of edge-sharing [FeO_6] octahedra are bridged by [$S1O_4$] tetrahedra through their corners. (c) Those dimers are linked via [$S2O_4$] tetrahedra in the (100) plane. This leads to a 3D structure with two types of channels along the c axis.[13] The low energy barrier associated with the transport of the sodium ions, especially Na3 in channel 2, was revealed by bond-valence sum analysis and by density functional theory calculations.[10,11]*

It was soon observed that, in practice, a sodium-rich $Na_{2+2x}Fe_{2-x}(SO_4)_3$ phase with $x \approx 0.25$ was obtained instead of the stoichiometric compound $Na_2Fe_2(SO_4)_3$.[4,12] The existence of a solid solution range stems from the partial occupancy of several sites in the alluaudite structure. Considering the general formula $[A(2)A(2)'][A(1)A(1)'A(1)''_2]M(1)M(2)_2[XO_4]_3$ proposed by Hatert et al. for the alluaudite structure, in NFS (Fig. 1) the octahedral M(2) site is occupied by Fe^{2+} and a small percentage of Na^+, the octahedral M(1) site is occupied by Na^+, and the remaining Na^+ partially occupy the [4 + 4]-coordinated distorted A(1) and A(2)' sites. The other A sites are empty.[1,13]

The off-stoichiometry in NFS was investigated as early as 2015 by Oyama et al.[4] They used samples with nominal composition $Na_{2+2x}Fe_{2-x}(SO_4)_3$ ($0 < x < 0.4$) prepared by solid state reaction at 350 °C starting from a ball-milled mixture of sodium sulfate and iron sulfate. An almost pure, off-stoichiometric alluaudite sulfate was obtained only for $x = 0.25$. Other compositions resulted in the formation of 5 to 15% of secondary phases. In a more recent study, Dwibedi et al.[14] prepared samples with Na/Fe ratios varying from 1 to 2 through an aqueous route with citric acid as a complexing agent and also concluded that formation of off-stoichiometric phases is favored. Following the work by Oyama et al.,[4]

Published in : Journal of Material Chemistry A (2019), vol. 14, pp. 8226–8233
DOI: 10.1039/C9TA00116F
Status : Postprint (Author's version)

stoichiometric NFS has been considered as a metastable phase and subsequent studies were performed on Na-rich compositions to minimize the presence of secondary phases.[2,4,8,9,14–24] However, this Na-rich phase contains a lower amount of the redox-active Fe ions, limiting the theoretical specific capacity to 106 mA h g^{-1} for $x = 0.25$.

Elucidating whether stoichiometric NFS exists or not is therefore an important issue, as highlighted in a recent review on polyanionic electrode compounds.[25]

The original NFS synthesis was carried out via a solid-state route, as described above.[1] Formation of the alluaudite phase proceeds through diffusion, during a heat treatment at relatively low temperatures (typically 350 °C) to prevent decomposition of the sulfates. Grain size reduction by ball-milling is used to decrease the length of the diffusion paths and the duration of the heat treatments,[1] but significant diffusion still needs to take place to form the final phase. Solution routes are a common strategy to create more homogeneous precursors and minimize diffusion lengths. However, in the case of NFS, precipitation in aqueous solutions results in the formation of inhomogeneous mixtures of $Na_2Fe(SO_4)_2{\cdot}4H_2O$ and iron sulfate,[15,26] while complexation with citric acid[14] does not prevent the formation of a Na-rich phase.

Here, we have built on information available about the individual sulfates to devise a synthesis strategy targeting a highly homogeneous cation distribution in the precursor. The successful preparation of stoichiometric NFS from a precursor prepared by reverse-strike coprecipitation in organic medium confirms that the homogeneity in the precursor is the key factor. We also validate the hypothesis of the metastable nature of the stoichiometric phase and investigate the structural and electrochemical differences between the stoichiometric and Na-rich phases.

EXPERIMENTAL SECTION

MATERIALS

$Na_2SO_4{\cdot}10H_2O$ (99+%) was purchased from Fluka, $FeSO_4{\cdot}7H_2O$ (99.5+%) and hydroquinone (99.5+%) were purchased from Acros. Water was obtained from a Milli-Q purification system. Isopropanol (99.8+%, HPLC grade) and glycerol (99.5%, bidistilled) were purchased from VWR. Water, isopropanol and glycerol were flushed with nitrogen to remove dissolved oxygen prior to their use. The water content of the sulfates was determined by thermogravimetric analysis.

SYNTHESIS

Samples with nominal compositions $Na_2Fe_2(SO_4)_3$ and $Na_{2.4}Fe_{1.8}(SO_4)_3$ (S samples and R samples, respectively) were synthesized via a precipitation method. In the optimized procedure (Scheme 1), 3.33 mmol (for R samples) or 2.5 mmol (for S samples) of $Na_2SO_4{\cdot}10H_2O$ and 5 mmol of $FeSO_4{\cdot}7H_2O$ were dissolved in 5 mL of water at 40 °C, into which 0.4 g of hydroquinone had been previously dissolved. This aqueous solution (A) was then added to 45 mL of glycerol at 60 °C and the resulting solution (B) was mixed for 5 minutes. Finally, solution B was added dropwise to 1 L of isopropanol at room temperature, under strong magnetic stirring, resulting in the formation of a greenish-white

Published in : Journal of Material Chemistry A (2019), vol. 14, pp. 8226–8233
DOI: 10.1039/C9TA00116F
Status : Postprint (Author's version)

precipitate. The precipitates were isolated by centrifugation, washed three times with fresh portions of isopropanol and dried under vacuum at room temperature overnight. These precursors were then heated for 2 h at 350 °C under flowing Ar with a heating ramp of 300 °C h^{-1}. The resulting samples are called S-2h and R-2h in the following sections.

All synthesized samples were kept in containers under an argon atmosphere to prevent hydration[27] of the sulfates.

Scheme 1 *Optimized procedure for the preparation of the NFS precursor (adapted from "Servier Medical Art" by Servier, used under CC BY)*

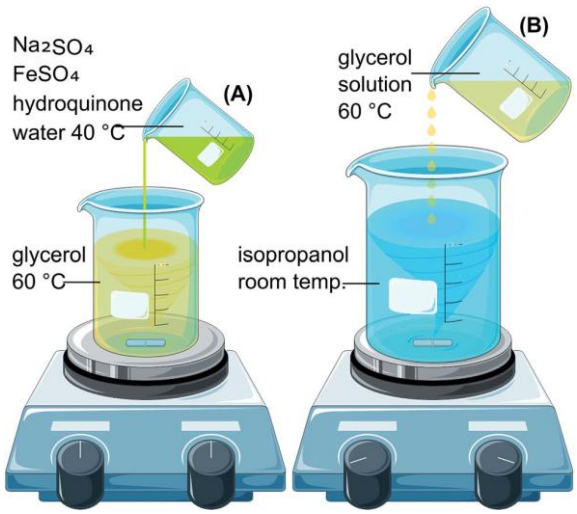

CHARACTERIZATION

The water content of the reactants was determined by thermogravimetric analysis using a Setaram LABSYS evo TGA 1150. The composition of the samples was assessed by inductively coupled plasma – optical emission spectrometry (ICP-OES) with a Varian spectrometer. The uncertainty on those measurements was estimated by propagation of the variances, assuming no correlation. It is reported as twice the standard deviation (95% confidence interval). The carbon content of the samples was determined using an Analytik Jena multiEA 4000 micro-elemental analyzer. The morphology and particle size were investigated by scanning electron microscopy (XL 30 FEG-ESEM, FEI).

Powder X-ray diffraction (XRD) was performed on a Bruker D8 diffractometer with a Cu-Ka radiation and a Lynxeye XE-T 1D detector (192 strips). Diffractograms were collected in the 10–130° 2θ-range with a 0.007° step size and a 2 s per strip step time. Operando XRD data (10–48° 2θ-range, 0.02° step size and 1.8 s per strip step time) were collected during electrochemical cycling in a specially designed cell with a beryllium window, using the same diffractometer and a Bio-Logic VMP3 galvanostat, at a rate of C/20. The cathode material was mixed with 20 wt% carbon black. The cell was mounted with a metallic Na counter-electrode, Whatman glass-fiber separators and a 1 M solution of $NaPF_6$ in propylene carbonate as the electrolyte. The XRD patterns were recorded every one hour in galvanostatic regime at C/20. Rietveld refinements of the diffractograms were conducted using the FullProf Suite,[28] in the C2/*c* spacegroup proposed by Barpanda et al.[1,16]

Published in : Journal of Material Chemistry A (2019), vol. 14, pp. 8226–8233
DOI: 10.1039/C9TA00116F
Status : Postprint (Author's version)

^{57}Fe Mössbauer spectra were acquired in transmission mode on a constant-acceleration spectrometer with a ^{57}Co(Rh) source at room temperature, in the ±12 mm s^{-1} and ±4 mm s^{-1} velocity ranges. The samples were prepared with about 30 mg of NFS material mixed with boron nitride. The spectrometer was calibrated using a high-purity *α*-Fe foil as a reference absorber. The spectra were fitted using Lorentzian doublets with the Fullham program to extract the hyperfine parameters. The quality of the fitting procedure was judged on the basis of minimizing the number of parameters and X^2 values.

Raman spectroscopy was carried out at room temperature using a confocal LabRam300 spectrometer (Horiba JobinYvon). Raman spectra were obtained at the surface of the sample powder. A 647 nm Krypton laser was used with a power density of 0.4 mW μm^{-2} on the sample. A higher power density leads to the degradation of the material by oxidation (as seen from the appearance of bands attributed to Fe_2O_3). The spectra presented in this publication were recorded during 40 s.

The electrochemical measurements were performed at room temperature with two-electrode Swagelok-type cells. The positive electrode mixture was prepared by gently grinding the active material with 10 wt% carbon black and 10 wt% polyvinylidene fluoride. The mixture was pressed on a stainless steel grid followed by drying in vacuum at 110 °C for 12 hours. Cells were assembled in an Ar filled glove box using a sodium Whatman glass-fiber separator, 1 M $NaPF_6$ dissolved in propylene carbonate as an electrolyte, and Na metal as counter and reference electrode. Galvanostatic cycling and cyclic voltammetry were conducted in a Bio-Logic VMP3 potentiostat.

RESULTS AND DISCUSSION

PRECURSOR DESIGN

As explained in the introduction, a solution route was designed in order to obtain a precursor homogeneous enough to yield stoichiometric NFS.

Since it is well known that ferrous ions readily oxidize in solution, all solvents were flushed with nitrogen and a small amount of hydroquinone was added to the sulfate solution to avoid Fe^{2+} oxidation. Hydroquinone was selected for its suitable reduction potential, its solubility in the selected solvents and its low boiling point,[29] and was found to have fast enough kinetics to suppress oxidation of Fe^{2+}.

Simple precipitation of an aqueous solution of sodium and iron sulfates into an organic solvent, such as ethanol, is known to yield a mixture of crystallized $Na_2Fe(SO_4)_2{\cdot}4H_2O$ and $FeSO_4{\cdot}4H_2O$;[15] we confirmed these results in the case of isopropanol. Due to the formation of a precipitate containing two separate phases, the benefits of the solution route are lost and the thermal decomposition of the $Na_2Fe(SO_4)_2{\cdot}4H_2O/FeSO_4{\cdot}4H_2O$ mixture yields a Na-rich NFS phase.[15]

Both sodium sulfate and iron(II) sulfate are reported to form dehydrated precipitates in water at temperatures above 32.4 °C[30] and 64.8 °C,[31] respectively. Therefore, the precipitation at 65 °C of an aqueous solution by isopropanol was investigated. However, in these conditions, the aqueous and organic phases are not miscible[32] and precipitation does not occur. Instead, the water in the aqueous fraction evaporates, leading to a mixture of $Na_2Fe(SO_4)_2{\cdot}4H_2O$ and $FeSO_4{\cdot}H_2O$.

Published in : Journal of Material Chemistry A (2019), vol. 14, pp. 8226–8233
DOI: 10.1039/C9TA00116F
Status : Postprint (Author's version)

To prevent the formation of $Na_2Fe(SO_4)_2{\cdot}4H_2O$, a non-aqueous route was developed based on a reverse-strike coprecipitation. Several solvents were considered (Table S4 in ESI). Glycerol was selected as the good solvent[33] and isopropanol as the bad solvent.[34] Glycerol was heated to about 60 °C to reduce its viscosity and enable a fast dissolution of the sulfates. The lower viscosity also facilitated the mixing of the glycerol solution with isopropanol during the precipitation, which was conducted by dropwise addition of the glycerol solution into a 20-fold larger volume of isopropanol. ICP measurements of the Na/Fe ratio in the precipitates showed that such a large excess of anti-solvent was necessary to reach quantitative precipitation.

During the procedure optimization, it was found that dissolving the sulfates in a minimum of water before diluting into glycerol was enough to prevent the formation of the $Na_2Fe(SO_4)_2{\cdot}4H_2O$ phase during precipitation, while allowing to dissolve a much larger amount of sulfates into solution. This optimized procedure is the one described in the Experimental section. It was applied to the synthesis of several batches and the phase formation after heat treatment (see hereafter) was consistent across batches.

PHASE FORMATION

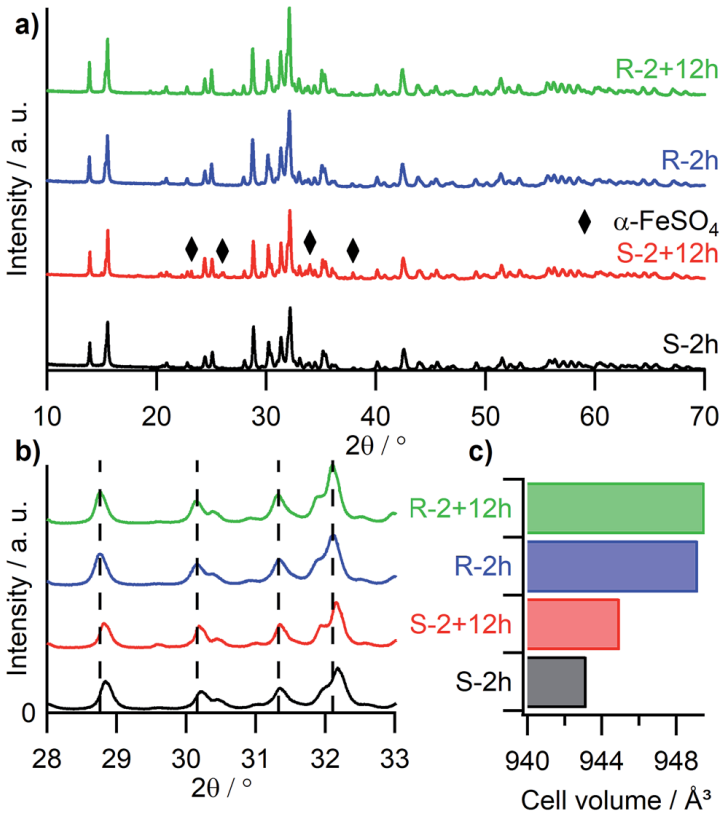

Fig. *2 X-ray diffraction data for the NFS samples. (a) X-ray diffractograms. (b) Close-up view of the diffractograms showing the shifts in the reflection positions. (c) Cell volume.*

Published in : Journal of Material Chemistry A (2019), vol. 14, pp. 8226–8233
DOI: 10.1039/C9TA00116F
Status : Postprint (Author's version)

A heat treatment of 2 hours at 350 °C in argon transforms the amorphous precursors into samples S-2h and R-2h. The X-ray diffractograms of S-2h and R-2h (Fig. 2a) show that in both cases all reflections can be indexed as single-phase alluaudite.

Some XRD reflections for the S-2h sample are shifted towards slightly higher angles in comparison with sample R-2h (Fig. 2b). The differences in cell parameters are reported in Table S1-1 in ESI. Fig. 2b also shows that the width of the reflections is similar for the two samples. If the sample contribution to the reflection width is interpreted as crystallite size broadening, the apparent crystallite size is 34 ± 2 nm for the S-2h and R-2h samples and increases slightly to 45 ± 5 nm after a further 12 h of heat treatment (S-2+12h and R-2+12h samples).

These XRD analyses show that no crystalline secondary phase can be detected after 2 hours at 350 °C. If an amorphous phase were formed, it would be expected to be a Fe-rich phase;[4] therefore, ^{57}Fe Mössbauer spectroscopy was used as a complement to X-ray diffraction. The Mössbauer spectra recorded at room temperature for the S-2h and R-2h samples (Fig. 3a and S2-1) are consistent with pure alluaudite phases, as shown by the satisfactory fitting with two Fe^{2+}-type doublets and hyperfine parameters (Table 1) in good agreement with those reported previously.[1] It can be concluded that the prepared phases are pure and that the Na/Fe ratios measured by ICP-OES (Table 2) correspond to the compositions of the alluaudite phases.

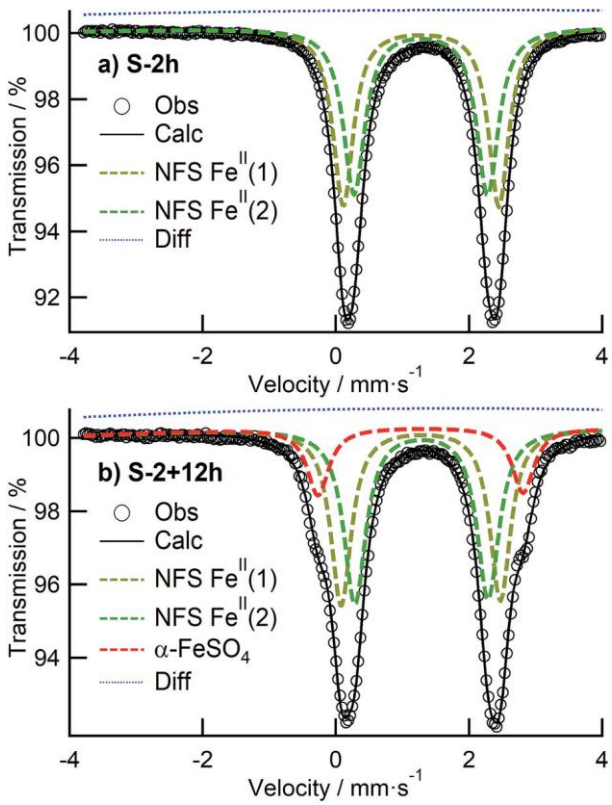

Fig. 3 *Room-temperature ^{57}Fe Mössbauer spectra of (a) S-2h and (b) S-2+12h.*

Published in : Journal of Material Chemistry A (2019), vol. 14, pp. 8226–8233
DOI: 10.1039/C9TA00116F
Status : Postprint (Author's version)

Table 1 *Hyperfine parameters[a] of the room-temperature ^{57}Fe Mössbauer spectra of R-2h and S-2h[a]*

Sample	Site	δ (mm s^{-1})	Δ (mm s^{-1})	Γ (mm s^{-1})	Area (%)
R-2h	$Fe^{II}(1)$	1.275(4)	2.43(1)	0.37(1)	50(1)
	$Fe^{II}(2)$	1.288(4)	2.06(1)	0.39(2)	50(1)
S-2h	$Fe^{II}(1)$	1.277(4)	2.34(1)	0.36(1)	50(1)
	$Fe^{II}(2)$	1.275(4)	2.01(1)	0.39(1)	50(1)

[a] δ, isomer shift referred to α-iron at 295 K; Δ, quadrupole splitting; Γ, line width.

Table 2 *Nominal and measured (ICP-OES) Na/Fe ratio in the samples*

	S sample	R sample
Nominal Na/Fe ratio	1.00	1.33
Nominal formula, $Na_{2+2x}Fe_{2-x}(SO_4)_3$	$Na_{2.00}Fe_{2.00}(SO_4)_3$, $x = 0.00$	$Na_{2.40}Fe_{1.80}(SO_4)_3$, $x = 0.20$
Measured Na/Fe ratio	1.08 ± 0.08	1.43 ± 0.09
Formula based on measured Na/Fe ratio	$Na_{2.10}Fe_{1.95}(SO_4)_3$, $x = 0.05 \pm 0.05$	$Na_{2.50}Fe_{1.75}(SO_4)_3$, $x = 0.25 \pm 0.05$

Since ^{57}Fe Mössbauer spectroscopy and ICP-OES provide information about the cations, Raman spectroscopy was used as a complementary technique to characterize other aspects of the samples. The Raman spectra of the S-2h and R-2h samples are shown in Fig. 4 and include a peak characteristic of the sulfate group at 1010 cm^{-1}. This peak occurs at the same position in both samples, suggesting that the sulfate group geometry is not significantly affected. This agrees with the Rietveld refinements of the XRD data. The Raman spectra also display the well-known D and G bands of carbon allotropes, at 1350 cm^{-1} and 1600 cm^{-1} respectively. The large width of the bands and their intensity ratio suggest that this carbon is amorphous,[35] which is consistent with the low temperature (350 °C) of the heat treatment in inert atmosphere. This carbon residue (about 4.5% according to carbon content analysis, see Table 3) results mainly from residues of the viscous glycerol solvent.

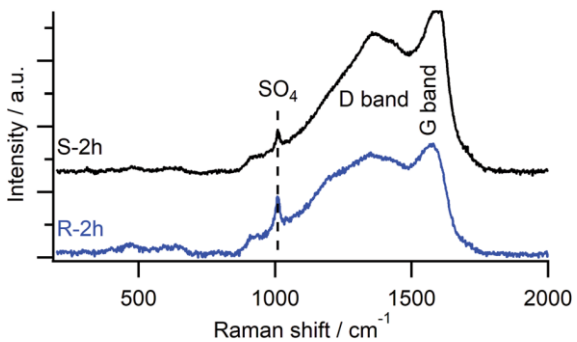

Fig. 4 *Raman spectra of the S-2h and R-2h samples.*

Table 3 *Carbon content in a precursor precipitate and in the samples after 2 h at 350 °C*

Sample	Precursor precipitate	R-2h	S-2h
Carbon content (wt%)	12.0(2)	4.5(1)	4.5(3)

Published in : Journal of Material Chemistry A (2019), vol. 14, pp. 8226–8233
DOI: 10.1039/C9TA00116F
Status : Postprint (Author's version)

Taken together, these results show that stoichiometric NFS exists and can be obtained by taking steps to promote the cationic homogeneity of the precursor. A further indication of this homogeneity in the case of the present samples is given by the fact that single-phase alluaudites can be obtained even if the temperature of the heat treatment is decreased to 200 °C. We performed this experiment following a recent report[14] of Na-rich alluaudite obtained via another wet route after 6 h at 200 °C. However, all the results reported hereafter were obtained on the samples treated at 350 °C.

PHASE STABILITY

In order to assess the thermal stability of the stoichiometric and Na-rich alluaudite phases, samples S-2h and R-2h were submitted to a further heat treatment of 12 h at 350 °C under argon. The X-ray diffractograms of samples S-2+12h and R2+12h are shown in Fig. 2 and their ^{57}Fe Mössbauer spectra in Fig. 3b and S2-1. As expected, the Na-rich phase is stable. On the contrary, the additional 12 h at 350 °C leads to the formation of a *α*-$FeSO_4$ secondary phase in the stoichiometric sample. Based on the surface areas and assuming equal recoil-free fractions of the different sites, the fit of the Mössbauer spectrum gives a proportion of 16% for this secondary phase (Fig. 3b and Table S2-1).

The absence of any iron-containing secondary phase in the Mössbauer spectrum of the original S-2h sample means that the iron sulfate diffused out of the stoichiometric phase during the additional 12 hours at 350 °C. This is confirmed by the evolution of cell volumes (Fig. 2c). The cell volume of S-2h is smaller than that of R-2h. As expected, the cell volume of R-2+12h is very close to that of R-2h. However, the cell volume of S-2+12h is intermediate between the S-2h and R-2h samples, indicating that it is transforming from the stoichiometric alluaudite towards a more Na-rich phase, the iron excess being ejected to form *α*-$FeSO_4$. This confirms the previously proposed hypothesis of a metastable nature of the stoichiometric NFS phase.

ELECTROCHEMICAL ACTIVITY

The synthesis method reported here yields large rod-like particles with lengths of a few micrometers and widths of a few hundreds of nanometers (Fig. 5). The rod-like particles form larger agglomerates, which do not favor efficient mixing with conductive carbon when processing the electrode mixtures. However the powder was not ground because, considering the metastable structure of the stoichiometric alluaudite, priority was placed on the preservation of the phase integrity.

Operando X-ray diffraction was used in order to confirm electrochemical activity in the stoichiometric alluaudite phase. The operando diffractograms for sample S-2h (Fig. 6) show that the material retains the alluaudite-type structure during Na^+ extraction/insertion. The peak shifts upon discharge correspond to a contraction of the cell volume, which provides evidence for the extraction of Na^+ ions. During the charge, the reflections return to their original positions, showing that the process is reversible. As better seen in Fig. 7, the whole intensity of the $(\bar{1}12)$ peak is shifted, confirming that all the material probed by the X-ray diffraction measurement is electrochemically active.

Published in : Journal of Material Chemistry A (2019), vol. 14, pp. 8226–8233
DOI: 10.1039/C9TA00116F
Status : Postprint (Author's version)

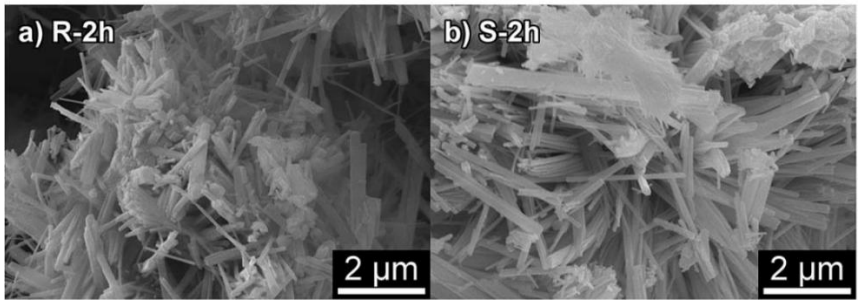

Fig. 5 *SEM micrographs of the (a) R-2h and (b) S-2h samples.*

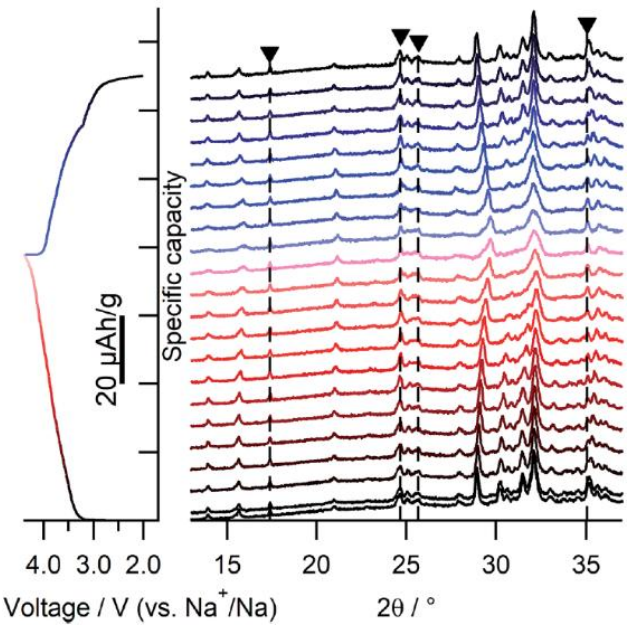

Fig. 6 *Operando X-ray diffractograms (right) along with the corresponding charge (red)/discharge (blue) curves (left) of S-2h. The ▼ symbol and the vertical dotted lines mark the peaks of the electrochemical cell (see Fig. S3-2 for more details).*

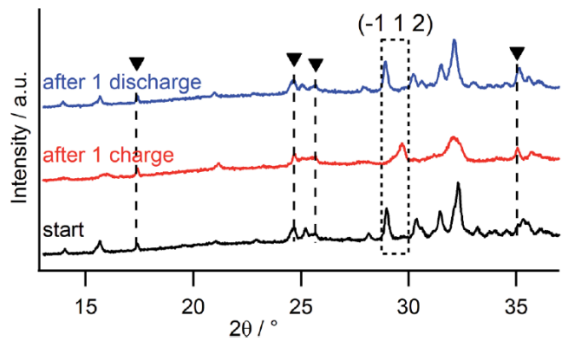

Fig. 7 *Operando XRD patterns of sample S-2h before cycling, after one charge and after one discharge. The ▼ symbol and the vertical dotted lines mark the peaks of the electrochemical cell (see Fig. S3-2 for more details).*

Published in : Journal of Material Chemistry A (2019), vol. 14, pp. 8226–8233
DOI: 10.1039/C9TA00116F
Status : Postprint (Author's version)

FURTHER ELECTROCHEMICAL CHARACTERIZATION

As a complement to the proof of electrochemical activity provided by the operando XRD results, we present in this last section some additional electrochemical characterization and further discussion about the impact of the less-than-optimal microstructure.

The galvanostatic charge/discharge curves presented in Fig. 8a are representative of the samples synthesized by the reverse strike co-precipitation method and show that the extraction/insertion of Na^+ ions occur in the same voltage range for the S-2h and R-2h samples. A cyclic voltammogram collected on sample S-2h is compared in Fig. 8c with published[1] differential galvanostatic profiles (dQ/dV) for a Na-rich $Na_{2+2x}Fe_{2-x}(SO_4)_3$ material. In both cases, the charge and discharge curves present three peaks, after the transitory first charge; the position of the discharge peaks is reproducible from the first to the second cycle. The results for S-2h are therefore consistent with the reported behavior for a sodium-ion alluaudite sulfate phase.

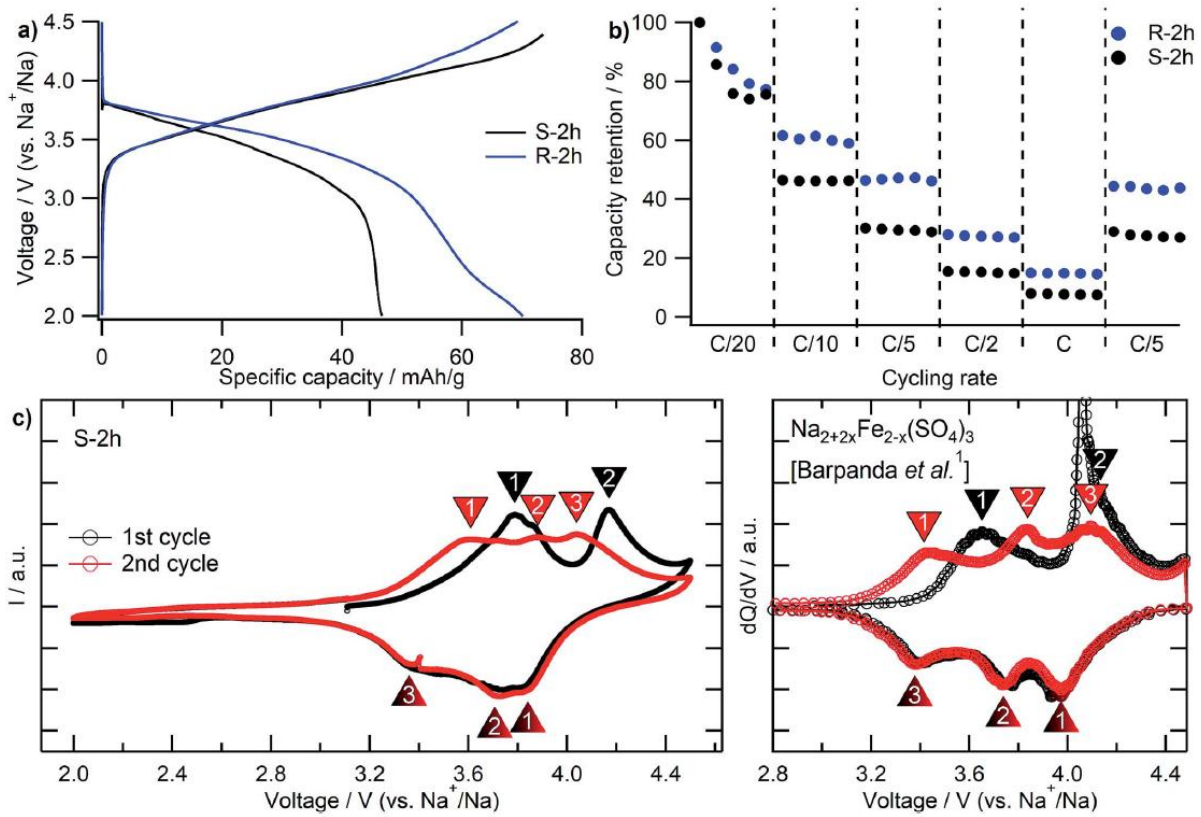

Fig. 8 *(a) Galvanostatic charge and discharge profiles of samples S-2h and R-2h between 2.0 V and 4.5 V at a rate of C/20. (b) Capacity retention upon cycling at various rates. (c) (left) Cyclic voltammetry of S-2h between 2.0 V and 4.5 V at a rate of 0.01 mV s^{-1} (right) differential galvanostatic profiles (dQ/dV) of $Na_{2+2}xFe_{2-x}(SO_4)_3$, adapted from Barpanda et al.[1] under CC BY 4.0. Triangles mark peak positions.*

Published in : Journal of Material Chemistry A (2019), vol. 14, pp. 8226–8233
DOI: 10.1039/C9TA00116F
Status : Postprint (Author's version)

However, the specific capacity values remain significantly lower than the theoretical capacities, even at low rate, and are amongst the lower range when compared with capacities reported in the literature. Besides, a significant capacity loss is observed when cycling at higher rate (Fig. 8b), which cannot be due to a degradation of the phase since the capacity recovers when the cycling rate is decreased again. We attribute this behavior to a low electric conductivity in the electrodes. As already noted, the large agglomerates revealed by electron microscopy (Fig. 5) are unlikely to mix efficiently with the conductive carbon additive. This hypothesis is further supported by the fact that results on electrodes from the same batch display a significant scattering of results.

The lower specific capacity is also observed in the case of the operando XRD experiment. These structural data provide additional information on the origin of the low practical capacity. As already noted for the S-2h sample (Fig. 7), the whole intensity of the $(\bar{1}12)$ peak is shifted during cycling, indicating that all the material probed by the X-ray diffraction measurement is electrochemically active at the low cycling rate. This is also true for the R-2h sample (see Fig. S3-1b). In the case of this Na-rich sample, comparison is possible with the synchrotron *in situ* diffraction study reported by Oyama *et al.*:[17] it turns out that the cell parameters extracted from our operando data for the R-2h sample (see Fig. S3-1a) are in good agreement with these reference data, confirming that the material probed by the X-ray diffraction measurement reaches complete charge/discharge. Since this probed material corresponds to the layer in closest contact with the current collector, this observation confirms the idea that microstructure-based issues of electron transport in the electrode play a major role.

CONCLUSIONS

The existence of stoichiometric NFS alluaudite has been demonstrated through its synthesis by a new reverse-strike coprecipitation route. The absence of secondary phases was ascertained by a combination of X-ray diffraction, ^{57}Fe Mössbauer spectroscopy and ICP-OES. According to Rietveld refinements, the stoichiometric phase has slightly different cell parameters and a smaller cell volume but no striking differences in the alluaudite structure were found. Further heat treatment leads to the decomposition of the stoichiometric phase into Na rich alluaudite and iron sulfate. These experimental results are consistent with the currently-held view that the stoichiometric alluaudite phase is metastable due to the repulsion induced by the short distance between Fe^{2+} ions in the Fe_2O_{10} dimers. The electrochemical activity of the Fe^{2+}/Fe^{3+} couple in the stoichiometric phase was confirmed through operando X-ray diffraction.

Our results should encourage a shift of the research effort on alluaudite sulfates towards (near)-stoichiometric compositions in order to benefit from the higher theoretical specific capacity.

The synthesis route followed in the present work was successfully designed to target cationic homogeneity in the precursors. Future work should focus on developing alternatives to meet the additional requirements of up-scalability and more favorable powder microstructures. The recent results of Chen *et al.*[36] suggest that their freeze drying route might be one of these alternatives, if the Na/Fe ratio of their alluaudite phase can be confirmed by accurate elemental analysis (such as ICP) and techniques sensitive to amorphous phases (such as Mössbauer spectroscopy).

Conflicts of interest

There are no conflicts to declare.

Acknowledgements

T. J. is thankful to F.R.S.-FNRS (Belgium) for a Research Fellowship, grant FC 17955. A. M. is grateful to the Walloon region for a Beware Fellowship Academia 2015-1, RESIBAT no 1510399. The authors are thankful to the University of Liège and F.R.S.-FNRS for equipment grants. Electron microscopy was performed at the CAREM platform (University of Liège).

† Electronic supplementary information (ESI) available: Results and experimental details on (S1) Rietveld refinements, (S2) Mössbauer spectra, (S3) operando X-ray diffraction and (S4) solvent selection. See DOI: 10.1039/c9ta00116f

References

1. P. Barpanda, G. Oyama, S. Nishimura, S.-C. Chung and A. Yamada, Nat. Commun., 2014, 5, 4358.
2. G. Oyama, H. Kiuchi, S. C. Chung, Y. Harada and A. Yamada, J. Phys. Chem. C, 2016, 120, 23323–23328.
3. L. Lander, J.-M. Tarascon and A. Yamada, Chem. Rec., 2018, 18, 1394–1408.
4. G. Oyama, S. Nishimura, Y. Suzuki, M. Okubo and A. Yamada, ChemElectroChem, 2015, 2, 1019–1023.
5. P. Barpanda, Isr. J. Chem., 2015, 55, 537–557.
6. S.-C. Chung, J. Ming, L. Lander, J. Lu and A. Yamada, J. Mater. Chem. A, 2018, 6, 3919–3925.
7. H. Ben Yahia, R. Essehli, R. Amin, K. Boulahya, T. Okumura and I. Belharouak, J. Power Sources, 2018, 382, 144–151.
8. S. Nishimura, Y. Suzuki, J. Lu, S. Torii, T. Kamiyama and A. Yamada, Chem. Mater., 2016, 28, 2393–2399.
9. J. Lu and A. Yamada, ChemElectroChem, 2016, 3, 902–905.
10. R. B. Araujo, S. Chakraborty, P. Barpanda and R. Ahuja, Phys. Chem. Chem. Phys., 2016, 18, 9658–9665.
11. L. L. Wong, H. M. Chen and S. Adams, Phys. Chem. Chem. Phys., 2015, 17, 9186–9193.
12. P. Barpanda, Chem. Mater., 2016, 28, 1006–1011.
13. F. Hatert, P. Keller, F. Lissner, D. Antenucci and A.-M. Fransolet, Eur. J. Mineral., 2000, 12, 847–857.
14. D. Dwibedi and P. Barpanda, MRS Adv., 2018, 3, 1209–1214.
15. Y. Meng, T. Yu, S. Zhang and C. Deng, J. Mater. Chem. A, 2016, 4, 1624–1631.
16. D. Dwibedi, C. D. Ling, R. B. Araujo, S. Chakraborty, S. Duraisamy, N. Munichandraiah, R. Ahuja and P. Barpanda, ACS Appl. Mater. Interfaces, 2016, 8, 6982–6991.
17. G. Oyama, O. Pecher, K. J. Griffith, S. Nishimura, R. Pigliapochi, C. P. Grey and A. Yamada, Chem. Mater., 2016, 28, 5321–5328.

18. R. P. Rao, H. Chen, L. L. Wong and S. Adams, J. Mater. Chem. A, 2017, 5, 3377–3388.
19. A. Goñi, A. Iturrondobeitia, I. Gil de Muro, L. Lezama and T. Rojo, J. Power Sources, 2017, 369, 95–102.
20. S. Wei, B. Mortemard de Boisse, G. Oyama, S. Nishimura and A. Yamada, ChemElectroChem, 2016, 3, 209–213.
21. J. Lu, S. Nishimura and A. Yamada, Chem. Mater., 2017, 29, 3597–3602.
22. T. Yu, B. Lin, Q. Li, X. Wang, W. Qu, S. Zhang and C. Deng, Phys. Chem. Chem. Phys., 2016, 18, 26933–26941.
23. W. Wang, X. Liu, Q. Xu, H. Liu, Y.-G. Wang, Y. Xia, Y. Cao and X. Ai, J. Mater. Chem. A, 2018, 6, 4354–4364.
24. D. Dwibedi, S. Baskar and P. Barpanda, ECS Trans., 2017, 80, 337–342.
25. P. Barpanda, L. Lander, S. Nishimura and A. Yamada, Adv. Energy Mater., 2018, 8, 1703055.
26. A. Seidell, Solubilities of inorganic and organic compounds; a compilation of quantitative solubility data from the periodical literature, New York, Van Nostrand, 1919.
27. M. Shishkin and H. Sato, J. Phys. Chem. C, 2017, 121, 20067– 20074.
28. J. Rodríguez-Carvajal, Phys. B, 1993, 192, 55–69.
29. CRC handbook of chemistry and physics: a ready-reference book of chemical and physical data, ed. D. R. Lide, CRC, Boca Raton, Fla, London, 88th edn, 2008.
30. L. Gmelin and R. J. Meyer, Natrium: Lieferung 3, Verlag Chemie., Berlin, 1966.
31. L. Gmelin and R. J. Meyer, Eisen: Teil B - die Verbindungen des Eisens, Verlag Chemie., Berlin, 1932.
32. A. L. Mills and F. A. Smith, Industrial & Engineering Chemistry Chemical & Engineering Data Series, 1957, 2, 30–31.
33. Glycerine Producers' Association, Physical Properties of Glycerine and Its Solutions, Glycerine Producers'Association, 1963.
34. F. K. Cameron, J. Phys. Chem., 1929, 34, 692–710.
35. A. Milani, M. Tommasini, V. Russo, A. L. Bassi, A. Lucotti, F. Cataldo and C. S. Casari, Beilstein J. Nanotechnol., 2015, 6, 480–491.
36. M. Chen, D. Cortie, Z. Hu, H. Jin, S. Wang, Q. Gu, W. Hua, E. Wang, W. Lai, L. Chen, S.-L. Chou, X.-L. Wang and S.-X. Dou, Adv. Energy Mater., 2018, 8, 1800944.